

*careful &
extensive*

**MILLIMETER WAVE LOSS IN
SUPERCONDUCTING STRIPLINES**

by

Chiyan Luo

**A thesis submitted in partial
fulfillment of the requirements for**

**Physics 78: Senior Thesis
Experimental**

California Institute of Technology

Thesis Advisor: Professor Jonas Zmuidzinas

Submitted May 4, 2000

California Institute of Technology

Abstract

MILLIMETER WAVE LOSS IN
SUPERCONDUCTING
STRIPLINES

by Chiyan Luo

Thesis Advisor: Professor Jonas Zmuidzinas
Department of Physics

The temperature dependence of the wave propagation in superconducting striplines from 80 to 100 GHz is experimentally examined for the first time. The measured resonance frequency spacing and temperature shift are in good agreement with theoretical predictions. The loss measurements are limited by SNR in the setup, and an upper limit of 0.01-0.02 of dielectric loss tangent is estimated near 80 GHz from 1.6K to 4.2K.

TABLE OF CONTENTS

List of Figures	ii
Acknowledgement.....	iii
Chapter 1: Introduction.....	1
Chapter 2: Basic Theory of Superconducting Transmission Lines.....	4
1. Basic Lossy Transmission Line Model.....	5
2. Anomalous Skin Effect.....	8
3. Superconductivity.....	10
4. Calculation Method Summary	12
Chapter 3: Experiments	13
1. Basic Idea.....	14
2. Basic Experiment: Setup.....	16
3. Basic Experiment: Results	19
4. Modified Experiment: Principle.....	21
5. Modified Experiment: Setup.....	24
6. Modified Experiment: Current Results	30
Chapter 4: Discussions and Conclusions	33
1. Implications of Two Experiments.....	33
2. Limitations of Current Modified Experiment	35
3. Conclusive Remarks and Future Work Direction	38
Bibliography.....	40

LIST OF FIGURES

<i>Number</i>	<i>Page</i>
2.1 Cross Section of a Superconducting Stripline: An Illustration.....	5
2.2 Derivation of Equations for Superconducting Stripline.....	7
3.1 Schematics of Gunn Oscillator System Setup	16
3.2 A Tested Device Chip for First Experiment	17
3.3 First Experiment Result.....	20
3.4 Output of Amplified Microwave Sources for a Typical Experiment	25
3.5 Modified Radiation Source Setup	26
3.6 New Mixer Block with Bias and Isolation Circuit	27
3.7 Measured IF Isolation without Chip	28
3.8 A Tested Device for Modified Two-Junction Experiment	29
3.9 Modified Experiment Setup Assembly	30
3.10 Modified Experiment Current Results	32
4.1 Simulation Fit of Basic Experiment Data	33
4.2 Simulation Fit for Modified Experiment Data.....	34
4.3 1.6K Data and Lock-in Noise Floor	36
4.4 Measured IF Channel Isolation with and without Chip.....	37

ACKNOWLEDGMENTS

The author is indebted to Professor Jonas Zmuidzinas for his numerous warm encouragements, for his help with actual device designs and for his valuable advice and insights on experimental methods. Henry LeDuc deserves the full credit for his beautiful work on SIS junctions and superconducting circuits fabrication. In addition, the author wishes to express his deep gratitude to David Miller for his patience and countless assistance with cryostat setup and with microwave laboratory. The author would also like to thank Jonathan Kawamura sincerely for his introduction and help to submillimeter laboratory and on various experimental details. Thanks also go to John Carlstrom for providing a waveguide filter near 80 GHz and Jeffrey Groseth for his quick installation of a helium pump.

Chapter 1

INTRODUCTION

Millimeter and submillimeter wave band of the electromagnetic spectrum, ranging from 100 GHz (3 mm) to 3 THz (0.1 mm), is an increasingly important part of observatory astronomy. Corresponding to radiations of thermal emission temperatures ($h\nu \approx kT$) from 4.8 K to 150 K, this band contains valuable information on interstellar dusts, on early stages of star formation within our galaxy, on far newly formed galaxies, on cosmic microwave background and on many other interesting topics in astronomy. A detailed and recent review of millimeter and submillimeter astronomy is given by Phillips and Keene (1992).

Much progress has been made in the detection of millimeter and submillimeter band for the past three decades. For broadband continuum observational needs, bolometers, which can respond to the total power of incident radiation, are developed as direct detectors. More frequently, for detection at higher resolutions in the spectral band, mixers and heterodyne techniques are employed. This detection scheme couples the incoming broadband signals to a strong laboratory radiation source of single frequency called the local oscillator (LO), and injects the resultant mixture into a nonlinear device called the mixer. Nonlinearity then produces signals at the difference frequencies called Intermediate Frequency (IF), which are typically at much lower frequencies and can be detected by routine methods. Along this direction, major success has been achieved on various different mixing elements, including hot-electron effect mixer, Schottky diode mixer and Superconductor-Insulator-Superconductor (SIS) mixer.

For frequencies below 700 GHz, the state-of-art detector of millimeter and submillimeter waves is SIS mixer, which offers near-quantum-limit low noise performance and high sensitivity, 5-10 times better than its hot-electron and Schottky counterparts (Carlstrom and Zmuidzinas 1996). At present time, much research is being carried out in many directions for further improvement of SIS detector performance. One such direction involves utilizing different superconductors of higher gap (e.g. NbTiN) for the SIS detector to extend the superconductor gap frequency limit above 700 GHz. Another major direction, however, is to design wide IF band and multi-channel SIS receivers, which is used as a submillimeter camera and capable of imaging the spectral distribution of an incoming signal in a much faster way. This direction also includes work to develop novel devices and integrated circuits for submillimeter wavelengths. All these research directions are based on knowledge on existing SIS technology.

A central question in all research on SIS devices is the coupling of RF signals to SIS junction. This is due to the fact that a SIS junction possesses some intrinsic geometric capacitance which is to be tuned out by some inductive circuits for maximal coupling purpose. An example of such a standard tuning circuit is discussed in detail by Bin (1997). The coupling is complicated by the additional requirement that the impedance of the transmission circuits should *match* those for receiving and for detection, since an unmatched circuit will produce undesirable reflection on the connecting ports and thus degrade the received signal. Modern lithography enables one to fabricate major components of a mixer, including the antenna, tuning circuits and SIS junction, on the same substrate. Although this technology possesses many advantages, such as guaranteed reproducibility and reliability, it has the drawback that the transmission lines and tuning circuits are not adjustable once it has been fabricated. Thus, knowledge on the basic properties of the transmission lines is highly desirable for future design and research work on SIS receivers. In fact,

lack of such knowledge already hindered the design of an existing quasi-optical slot antenna SIS mixer (Zmuidzinis and LeDuc 1992).

This thesis describes a first experimental effort to determine one of the fundamental properties of the niobium superconducting striplines, namely the attenuation constant, at millimeter wavelengths from 80 GHz to 100 GHz. Previous experimental data on the loss of superconducting transmission lines at millimeter and submillimeter wavelengths are scarce, mainly due to lack of instrumentation in this range. Whitaker et al (1988) did some work in ultrafast signals (10^{11} to 10^{13} Hz) on superconducting striplines, but their data reflects only collective wideband behavior of the stripline and mainly concerns with the transmission phase velocity, not the precise loss. Although more data and various experimental methods are available at lower frequencies in the microwave range, (Popel 1983, Turneure et al 1968, Langley et al 1991), their testing frequencies are not of interests to current radio astronomy. Thus the experiments in this thesis work are pioneering work. The phase velocity of millimeter waves on such transmission lines obtained from this work, although of less interests, are also in good agreement with the calculations on which previous mixer designs were based. This work is also our first step toward measuring the loss in Nb/SiO/Nb superconducting striplines near 500 GHz and determining whether or not a novel device based on the sharp temperature dependence of the superconductor loss would be actually feasible.

The organization of this thesis is as follows. Chapter 2 describes the basic theory of superconducting striplines. Chapter 3 discusses the main ideas of the experiment, the actual experimental setups and current obtained data. Chapter 4 outlines the implications of present results and presents the conclusions of this thesis.

Chapter 2

BASIC THEORY OF SUPERCONDUCTING TRANSMISSION LINES

Below 700 GHz, the on-chip tuning circuits of the SIS mixers are transmission lines made from the superconductor Niobium which has a superconducting transition temperature of 9.2 K. Typically these transmission lines have a thin dielectric layer made from silicon monoxide (SiO) which is sandwiched between two thin superconductive layers of niobium, with roughly the same thickness for all layers ($\sim 200\text{nm}$). Due to lack of knowledge about the real behavior of these transmission lines, initial mixer designers relies on theoretical models to simulate their properties in the frequency range of interest. These models are experimentally tested in previous mixers to be applicable in crude approximation. Simulation systems and libraries which are capable of the calculations used in these models have been developed and are now readily available, such as *Supermix* (Ward et al) in C++. These computer programs enable one to design mixers and superconducting circuits and to interpret experimental data without the need to refer to the underlying theory and to locate the exact formula. In fact, the data obtained in this thesis work are analyzed in Chapter 4 using these computer programs. Nevertheless, a thorough understanding of the basic theory of the superconducting transmission lines is still essential for future research work on refinements and improvements of these devices, and is the key foundations of the experiments in this thesis work. Therefore, in this chapter the current theoretical models are briefly reviewed, and the methods for calculation with the experimental data are explained.

! (honest
↓
direct!)

1. Basic Lossy Transmission Line Model

In this section we will review the basic lossy transmission line model from a physical point of view. Consider a segment of transmission line as that described in the last section carrying a millimeter wave with angular frequency ω . Let z axis point toward the direction of wave propagation and x axis point perpendicular to the metal-dielectric interface. The x - y plane defines a cross section of the transmission line. The geometry of the layers is specified in Figure (2.1), and the problem is to determine the wave propagation in this line.

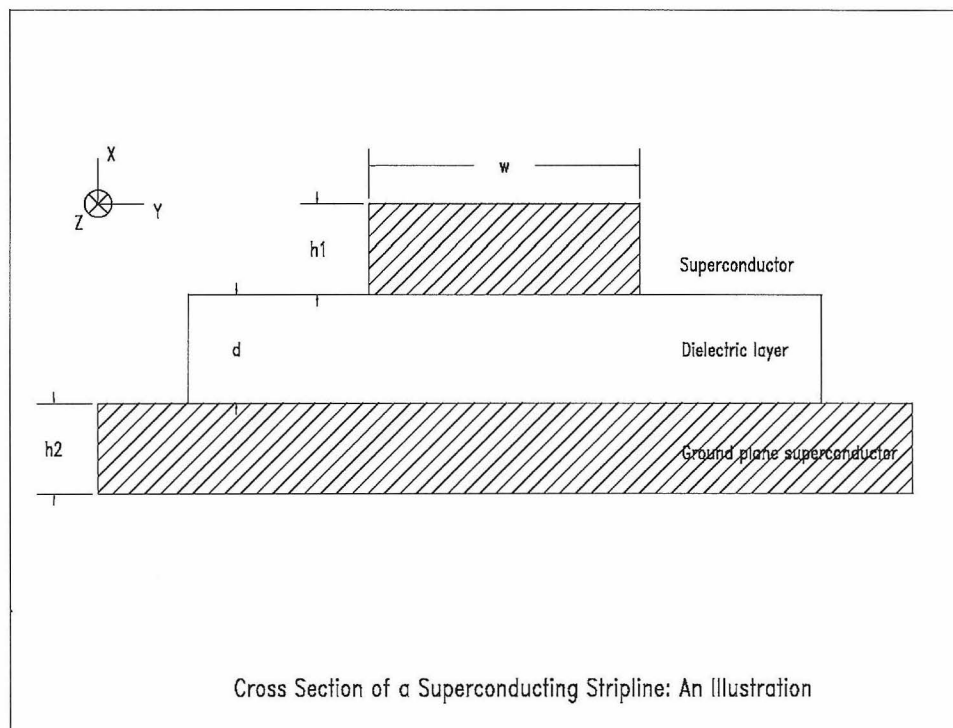


Figure 2.1 Cross Section of a Superconducting Stripline: An Illustration

We will only consider this problem approximately in the parallel plate limit $w \gg h_1, h_2$, and ignore radiation losses and surface roughness effects. Let the dielectric constant of the dielectric layer be ϵ , and let all layers have vacuum

magnetic permeability μ_0 . Without loss, the electric field \mathbf{E} becomes strictly perpendicular to the metal-dielectric interface. The traveling wave solutions are then obtained:

$$\mathbf{E} = E_0 \exp(\pm i(kz - \omega t)) \hat{\mathbf{x}} \quad \text{and} \quad \mathbf{H} = H_0 \exp(\pm i(kz - \omega t)) \hat{\mathbf{y}} \quad (2.1)$$

where $k = \omega \sqrt{\mu_0 \epsilon}$ and $H_0 = \sqrt{\frac{\epsilon}{\mu_0}} E_0$.

When we begin to consider RF loss in the superconductors, the problem becomes fairly involved as will be explained in the next sections. In this section, the metal layers is assumed to be described by a surface impedance:

$$Z = \frac{E_{//}}{H_{//}} = R - iX \quad (2.2)$$

where R is the *surface resistance* and X is the *surface reactance*, and $\mathbf{E}_{//}$ and $\mathbf{H}_{//}$ are fields parallel to the metal surface and perpendicular to each other. (2.2) are actually derived when waves are traveling perpendicular to the metal surface, but we will assume that it holds to first order in Z for our problem.

Now the zeroth order solution has a magnetic field component along y-axis, which, according to the definition surface impedance, will induce a small electric field component along the direction of $\hat{\mathbf{n}} \times \hat{\mathbf{y}}$, where $\hat{\mathbf{n}}$ is the unit vector pointing perpendicularly outward the metal surface. Since this small electric field is along the z-axis, we can take a loop in the xz-plane (cf. Figure 2.2) and apply the Maxwell equations around that loop in the limit that Δx goes to 0 to obtain:

$$\frac{dE_x}{dz} = i\mu_0 \omega H_y - \frac{2Z}{d} H_y \quad (2.3)$$

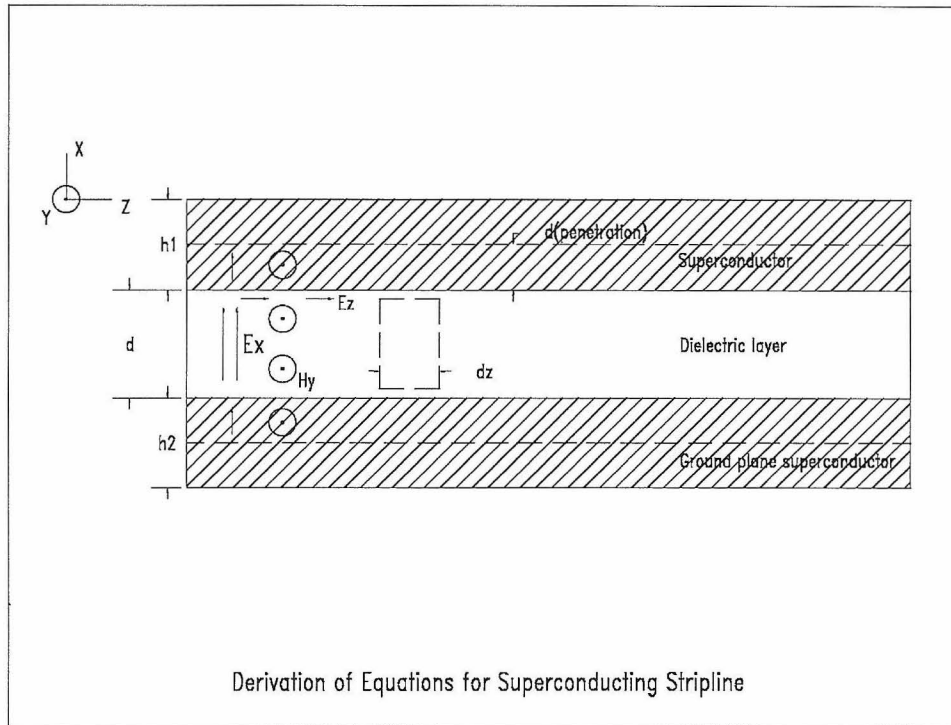


Figure 2.2 Derivation of Equations for Superconducting Stripline

A similar consideration of Maxwell's equations in a small loop in yz-plane yields

$$\frac{dH_y}{dz} = i\epsilon\omega E_x \quad (2.4)$$

where $\epsilon = \epsilon_0\epsilon_r(1 + i\tan(\delta))$ and $\tan(\delta)$, called the loss tangent, represents the loss in the dielectric of the transmission line. Equations (2.3) and (2.4) form the system that governs the propagation of wave on a lossy transmission line. Compared to corresponding expressions in lumped-element circuits, (2.3) and (2.4) also explain why transmission lines are often modeled as a ladder of series

impedances (inductors and resistors) and shunt admittances (capacitors and conductors) in electrical engineering.

We can eliminate H_y from this system and obtain:

$$\frac{d^2 E_x}{dz^2} + \beta^2 E_x = 0 \text{ with } \beta^2 = \mu_0 \epsilon \omega^2 + \frac{2i\epsilon\omega Z}{d} \quad (2.5)$$

Since β is generally a complex number, equation (2.8) represents a travelling wave along z axis with damping amplitude. The real part of β represents the phase propagation of EM wave, while the imaginary part of β stands for the attenuation constant.

While the loss in this transmission line is small, i.e. $\frac{\text{Im}(\beta)}{\text{Re}(\beta)} \ll 1$, we can solve for β to first order in the losses from (2.8) and obtain:

$$\text{Re } \beta \approx \sqrt{\epsilon_r} \frac{\omega}{c} + \frac{X}{d\mu_0\omega} \text{ and } \text{Im } \beta = \frac{\sqrt{\epsilon_r}\omega}{2c} \tan \delta + \frac{R}{d} \sqrt{\frac{\epsilon_0}{\mu_0}} \quad (2.6)$$

where c is the speed of light in the vacuum. These equations show that the wave propagation on these transmission lines is affected by the surface impedance and the dielectric loss, a result which can be compared to experiments.

2. Anomalous Skin Effect

When we begin to take into account the loss in the system, this problem is complicated in two folds. First of all, niobium is a superconductor which has drastically different electrodynamic properties from conventional conductors. This is reviewed in section 3. Second of all, there may be the so-called *anomalous*

skin effect in our experimental conditions, for reasons that are explained briefly in this section.

At lower frequencies, the EM field penetrates into the metal only in a small distance called the skin depth. In classical theory, the key equation that leads to this property of metals is the classical Ohm's law,

$$\mathbf{J}(\mathbf{r}) = \sigma \mathbf{E}(\mathbf{r}) \quad (2.7)$$

which predicts a local and immediate response current of the metal to the external fields. This is because in deriving (2.7) a constant electric field over the mean free path of the conducting electrons is assumed. However, as frequency goes up and temperature goes down, the classical skin depth will decrease and the mean free path of the conduction electrons will increase, so that the skin depth may be much smaller than the mean free path. In this case a local relation such as (2.7) which is derived neglecting the spatial variance of $\mathbf{E}(\mathbf{r})$ can be violated.

A calculation in the non-local regime can be hard since the complicated boundary conditions at the metal surface will necessarily come into play. A standard treatment is to first derive the kernel for non-local electrodynamics (i.e. the relation between \mathbf{J} and \mathbf{E} when both have harmonic space-time dependence), and then solve the boundary value problem using this kernel. In normal metals, the first step was achieved via semiclassical methods by Pippard and Chambers (c.f. A. B. Pippard 1965) and via quantum mechanical perturbation theory by Mattis and Bardeen (1958). The second step is solved classically by Reuter and Sondheimer (1948), but no quantum mechanical solutions have yet been accomplished.

Fortunately, for the experimental conditions described in this thesis, the niobium films has a relatively high normal resistivity which puts an upper limit on

the mean free path of its conducting electrons. If the experimental frequency is near 100 GHz, then the mean free path and the classical skin depth is about the same order of magnitude. In this case a local theory gives results that deviate only slightly from those in an anomalous theory. For simplicity, therefore, in this experiment calculations are done in the local limit.

3. Superconductivity

The standard microscopic theory of superconductivity goes back to the classic 1957 paper by Bardeen, Cooper and Schrieffer. In their paper, BCS put forth the model in which electrons with antiparallel spins condense into pairs by exchange of virtual phonons, and all pairs are phase-coherent in the ground state. A finite amount of energy is required to break a pair into quasi-particles, a key feature as demonstrated in the BCS theory. In DC conduction, all pairs are carrying the same total momentum and thus participating in conduction simultaneously. The probability of scattering off a significant portion of the electron pairs is extremely small, and therefore in BCS phase DC conduction can persist indefinitely. For AC conduction, however, energy is required to shift the energy levels the thermally excited normal electrons, and therefore a superconductor will display some real *resistance* in AC conduction, apart from its apparent inductive behavior due to acceleration of virtual electron pairs.

Mattis and Bardeen (1958) derived a complete non-local expression for anomalous skin effect in superconductors. For our purposes, we only need to use the kernel of his expression, as an approximation. Our *local* relations will thus be (Kautz 1978):

$$\frac{\sigma_1}{\sigma_n} = \frac{2}{\hbar\omega} \int_{\Delta}^{\infty} dE [f(E) - f(E + \hbar\omega)] \frac{E^2 + \Delta^2 + \hbar\omega E}{\sqrt{E^2 - \Delta^2} \sqrt{(E + \hbar\omega)^2 - \Delta^2}}$$

$$+ \frac{1}{\hbar\omega} \int_{\Delta}^{\hbar\omega-\Delta} dE [1 - 2f(\hbar\omega - E)] \frac{\hbar\omega E - E^2 - \Delta^2}{\sqrt{E^2 - \Delta^2} \sqrt{(E - \hbar\omega)^2 - \Delta^2}} \quad (2.8)$$

$$\frac{\sigma_2}{\sigma_n} = \frac{1}{\hbar\omega} \int_{\Delta-\hbar\omega, -\Delta}^{\Delta} dE [1 - 2f(\hbar\omega + E)] \frac{\hbar\omega E + E^2 + \Delta^2}{\sqrt{E^2 - \Delta^2} \sqrt{(E + \hbar\omega)^2 - \Delta^2}} \quad (2.9)$$

where $f(E) = \frac{1}{1 + \exp(\frac{E}{kT})}$ is the Fermi distribution function, Δ is the

superconducting energy gap, and σ_n is the normal conductivity. The first integral in (2.8) represents AC conduction of thermally excited normal electrons, and the second integral represents AC excitation of quarsi-particles by the EM field. The second integral is zero if $\hbar\omega < 2\Delta$. (2.9) describes the acceleration of superelectrons by RF field. If $\hbar\omega < 2\Delta$ the lower limit of the integral in (2.9) is $\hbar\omega - \Delta$; otherwise the lower limit is $-\Delta$. Our expression for the superconductor's electrodynamics will then be:

$$\mathbf{J}(\mathbf{r}) = (\sigma_1 + i\sigma_2)\mathbf{E}(\mathbf{r}) \quad (2.10)$$

which is used to replace (2.7) in the transmission line theory. Thus, the surface impedance can be calculated just as in classical theories, with the conductivity changed to the Mattis-Bardeen expression.

Although the loss predicted by (2.8) is real, in Nb striplines it is quite small below 700 GHz, twice the niobium superconducting gap frequency. Since the population of thermally excited normal electrons roughly scales as $\exp(-\frac{2\Delta}{kT})$, we expect the surface resistance decreases quickly as T goes down. In fact, according to the Mattis-Bardeen theory, the loss in the superconductor is a strong function of temperature, and the superconductor will become perfectly lossless at

0K at any frequency. The principal interests in this thesis work derive from this observation. Indeed, as shown in (2.6), if the loss in the dielectric is negligible, then the loss in the superconducting striplines will also be a strong function of temperature and hence be measurable.

4. Calculation Method Summary

The actual calculations of the experimental data in Chapter 4 of this thesis are carried out using the C++ library *Supermix* developed in the Submillimeter Astrophysics Group at California Institute of Technology. This library contains classes that can simulate actual devices and calculate their properties if the device parameters are provided. Most importantly, this library calculates the superconductor surface impedances using the Mattis-Bardeen theory in the local limit and simulate the performance of superconducting striplines in the manner described in this chapter. Using this library, one only needs to specify the superconductor and dielectric layers and their parameters and stripline width and length in a C++ code program, and the class methods defined in the library will give all characteristics of the stripline. One can further integrate antenna circuits, RF chokes and transformers altogether in the code, and the resulting program can thus simulate the performance of the full on-chip circuit directly. Thus, no explicit surface impedance calculations and Mattis-Bardeen integrals will be presented in this thesis. We will instead present the results of such calculations and compare them with experimental data in Chapter 4.

Chapter 3

EXPERIMENTS

The major experimental difficulties presented in measuring the loss in the superconducting transmission lines are two-fold. On the one hand, there are some general obstacles in measuring small signals. Since the predicted loss is quite small, a direct measurement, which measures the absolute magnitude of the destructive combination of the attenuated signal with the incoming signal, is desirable. Some interference pattern should be constructed in turn. However, this technique requires that the power source used for this measurement must be fairly clean and stable. As will be discussed below, a tunable Gunn Oscillator which operates from 90 to 110 GHz under phase lock proves to be not clean enough in one of our previous measurement. Its $3/2$ harmonic output mode is only expected to be -10dB smaller and hence can be interfere with the main harmonic when the response is smaller than -10dB. Thus some modifications to the existing RF power supply are required, or alternative power sources need to be found. On the other hand, within our current quasi-optical detection scheme the coupling efficiency is always subject to unknown influences along the optical pathway of the signal. Given the consideration that the received signal is potentially fluctuating due to changing experimental environment, it would be necessary to be able to measure the received signal during the experiment. This also requires some changes to our detector system. In this chapter the actual experimental methods to circumvent these practical difficulties are described in detail, and the results are briefly presented.

1. Basic Idea

In order to measure the surface resistance accurately, we choose to do a resonator experiment, in which we superpose the incoming wave and the attenuated wave to form interference. We implement this idea naturally by an open-ended transmission line which is a perfect reflector for the incoming signal at all frequencies. When the standing wave resonance is formed, the incoming wave and the attenuated wave add in opposite phase, which results in a signal that scales with the attenuation. If the superconductors and dielectric were without loss, then the reflected wave would not be attenuated in its amplitude and the destructive interference will produce absolute zero. Accordingly, by measuring the depth of the nulls at the destructive interference it is possible to determine the loss in the transmission lines.

To simplify the design and the measurements, we choose to fix the resonator stub length, l , that we are interested in and vary the frequency of the radiation, f . Let the EM propagation constant on transmission lines be (cf. (2.6)):

$$\beta = k + i\alpha \quad (3.1)$$

where $k = \frac{2\pi f}{c'}$ and c' is the speed of light on the transmission lines. Then the amplitude of the reflected wave has an additional factor of

$$\begin{aligned} \exp(i2\beta l) &= \exp(-2\alpha l) \exp(i2kl) \\ &= \exp(-2\alpha l) \exp(i \frac{4\pi fl}{c'}) \end{aligned} \quad (3.2)$$

relative to the incoming wave. Therefore, when this wave is superimposed on the incident wave at a fixed length l and varying frequency f , we would expect to see

resonance structures at frequency interval $\Delta f = \frac{c'}{2l}$. The depth of the destructive nulls in *power* response can be estimated to be

$$\left(\frac{1 - \exp(-2\alpha l)}{1 + \exp(-2\alpha l)}\right)^2 \approx \left(\frac{1 - (1 - 2\alpha l)}{2}\right)^2 = \alpha^2 l^2 \quad (3.3)$$

when compared to the peak value. Hence the null depth is directly a measure of the superconducting loss at submillimeter wavelengths.

With the existing technology of planar fabrication and sensitive SIS detectors, measuring such resonances becomes very possible in a tabletop experiment. The main experimental efforts in this thesis work are therefore directed toward constructing up the measuring system in a home laboratory and measuring the resonance curves. Currently, two different experimental setups have been tried at the millimeter wavelength (80 GHz – 100 GHz), which are respectively described in the following sections.

2. Basic Experiment: Setup

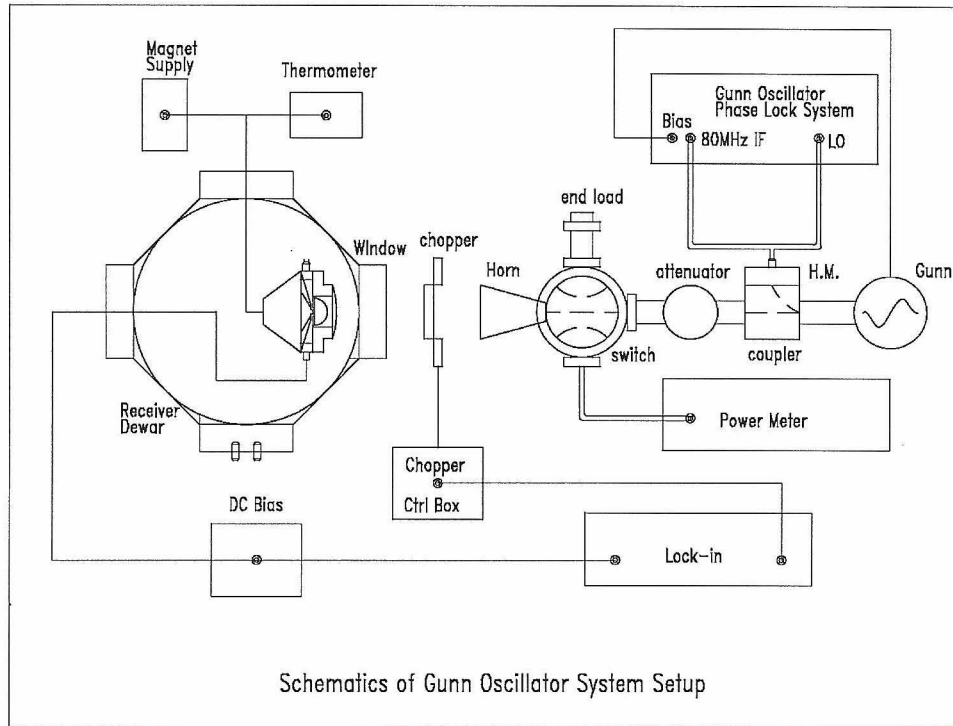


Figure 3.1: Schematics of Gunn Oscillator System Setup

The first experiment was done using a design for SIS mixers similar to that described by Zmuidzinas and LeDuc (1992). Here, SIS junction is placed a distance $l = 10.0\text{mm}$ from the open-ended niobium microstrip line, with a junction area $A = 2\mu\text{m} \times 2\mu\text{m}$. Radiation is coupled to this resonator from a two-slot antenna by a section of transmission line which is also used to match the impedances between the antenna and the microstrip. The twin-slot antenna is built on a thick niobium ground plane. High frequency radiation energy is confined within the transmission lines and the ground plane via large-area radial stubs serving as RF short circuits. In this way, DC bias can be applied to the SIS junction to place on it an appropriate operating voltage, but RF signals cannot leak out to the biasing electronic circuits. The whole system is planar, and is

fabricated on a $3.14\text{mm} \times 2.14\text{mm} \times .39\text{mm}$ silicon substrate. A real life picture of a tested device is shown below in Figure 3.2.

This chip is then mounted on the flat silicon disk on the back of a hemispherical silicon lens, which resides in a $50.8\text{mm} \times 38.2\text{mm} \times 15.0\text{mm}$ gold-plated mixer block. The biasing of the SIS junctions is achieved by a six-wire measurement circuit mounted inside the mixer block which can measure the voltage and current bias on the junction. A coil is also attached to the back of the mixer which can produce a magnetic field through the junctions to suppress noise due to the junction's Josephson current. This mixer block is in direct metallic contact with the cold plate of the cryostat, and all bias circuits on it are wired out to the outer jacket of the cryostat after heat sinking to the 77 K shield.

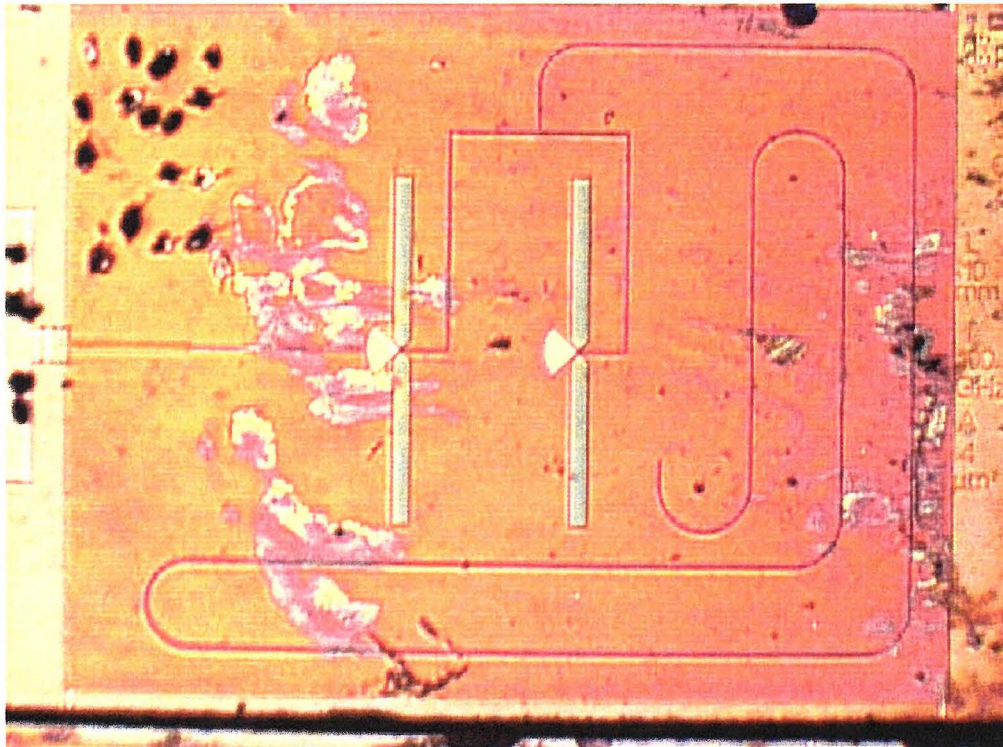


Figure 3.2: A Tested Device Chip for First Experiment

During this first experiment, a H122 Gunn Oscillator is used as the radiation source. This Gunn Oscillator can be manually set to an arbitrary frequency between 90 and 110 GHz using an existing phase-lock system, in the manner as described by Carlstrom et al (1985). This radiation is injected into the mixers inside the cryostat via quasi-optical coupling scheme, and a plastic lens is used outside the dewar to refocus the diverging output pattern of the WR-10 horn into a slowly converging beam as designed for the mixer system. To reduce the random noise at DC detection, a wheel-chopper is used to chop the incoming radiation, and by locking to the frequency of the chopper on a lock-in amplifier (Stanford Research Systems, Model SR510) a signal of modest strength can be detected with an appreciable SNR (usually of order 10^2 in the amplitude ratio).

Since the Gunn Oscillator can output a fair amount of power (usually ~ 100 μW between 90 GHz and 100 GHz), for convenience a direct detection scheme is used. According to Tucker's Theory for SIS detectors (Tucker and Feldman 1985), a SIS junction under constant voltage bias can produce a DC current on top of its leakage current in response to an external millimeter wave radiation. When the signal strength is small, small-signal approximation indicates that this current should be proportional to the *power* of the external driving force. Therefore, using the SIS junction as a direct detector the power transmitted to the junction via the open-ended microstrip can be measured by reading the voltage value on the lock-in. Moreover, the power injecting into the cryostat window is in proportion to the power coming out of the horn, assuming the quasi-optical coupling has a constant efficiency with respect to frequency. Thus the incoming power can also be measured using a 100 GHz waveguide sensor and a power meter at the source. For convenience, a waveguide switch is inserted to enable the horn power and the detected power be measured at the same time.

To maintain maximal signal-to-noise ratio during the measurement, in the first experiment the power level injected into the mixer is manually varied by adjusting an attenuator before the switch, so as to maintain almost constant signal strength at the output lock-in. With the power meter connected to the other port of the switch, the bookkeeping of the power can be done. This method has the additional advantage of broad dynamic range, since the power meter can measure the millimeter radiation as small as $5 \mu\text{W}$ and as big as 5mW , thus allowing 30 dB of dynamic range without sacrificing SNR significantly. Of course, this method relies heavily upon the assumption that the quasi-optical coupling is constant from the output of the horn all the way to the connection port between the twin-slot antenna and the tapered microstrip lines, constant at all frequencies and power levels used in the experiment. All the variations of the ratio of the signal to the incident power are thus attributed to the interference pattern on the open-ended microstrip line. This assumption is based on previous successful Fourier Transform Spectroscopy measurements on the current detector system using flat beam black body radiation sources, and its validity in the current setup is yet to be established.

3. Basic Experiment: Results

In this experiment devices from Batch L990319.01 are used. The SIS junctions have a junction area $A \sim 4 \mu\text{m}^2$ and have integrated twin-slot antenna designed for 100 GHz. At liquid helium temperature, they show good I-V curve response: $\sim 2.81 \text{mV}$ superconducting gap voltage (corresponding to $\Delta \approx 1.4 \text{meV}$), $\sim 5.7 \Omega$ normal resistance, and a subgap to normal ratio of roughly 20. The junction is biased at 2.20mV . Measurements of the stub resonator transmission are carried out first at liquid helium temperature 4.2 K, and then at 1.7 K by reducing the vapor pressure above the liquid helium. The junction dark current drops from $55\mu\text{A}$ to $31\mu\text{A}$. The phase-lock system for Gunn Oscillator

and the switch is current not automated, and the whole experiment is carried out manually. One of the best-measured original data is plotted in the following figure.

Clearly one null around 92 GHz comes out fairly cleanly. The dramatic increase of the depth of the null with the reduction in temperature seems to imply the expected strong temperature variation of superconductor losses. However, some serious problems are also obvious in this plot. No clear periodic structures are observable here, and signals above 94 GHz appear to be unsmooth and without the correct frequency shift as temperature goes down.

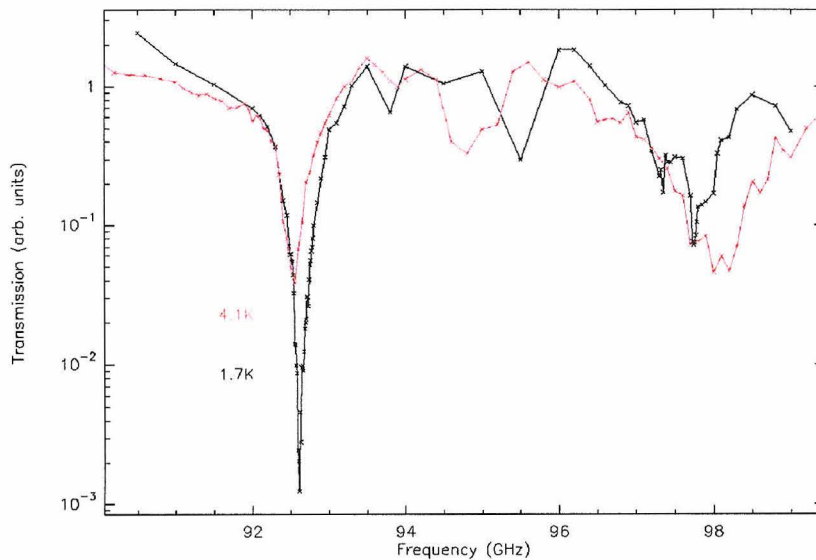


Figure 3.3: First Experiment Results

Many causes are possible for this wild behavior. One likely reason is that the Gunn Oscillator can output not only the principle frequency mode as set by its

tuning and backshort knobs, but also a higher $3/2$ frequency mode in its resonance cavity. Although this side band is usually at least -10 dB less in power than the principle mode, it is possibly present and interferes with measurements above 95 GHz. Another potential reason is that there may be some obstacles in the quasi-optical paths of our receiver which can produce some unknown effect to the response. Both of these speculations are difficult to investigate further since there is no suitable filter or calibration meter inside the cryostat available in the laboratory.

The difficulties here are exactly the ones mentioned at the beginning of this chapter. To overcome these difficulties, a very clean radiation source near the 100 GHz band and a very accurate power calibration system are both highly desired. This is where the main efforts of this thesis work are devoted and will be discussed in the following several sections.

4. Modified Experiment: Principle

Our first experiment shows that it is necessary to use a clean millimeter/submillimeter radiation source, as well as to perform careful power calibration in order to complete precision measurements in the microstrip lines. The entire experiment setup is thus modified in observance of these two requirements. Simply speaking, the radiation source is changed to phase-lock detection at the final signal port instead of at the source output, and a second SIS junction is used on-chip to monitor any power level fluctuations. Due to these changes we have effectively also modified the basic receiver principle. For completeness, the modified detection principles are reviewed here.

In the new experiment we are directly using the radiation from harmonic mixers as our radiation source. These harmonic mixers can accept microwave signals of lower frequency (between 10 and 20 GHz) and output a series of

coherent millimeter waves that are of exact integer multiples of the input signals. In order to keep track of the exact harmonic number of the signal that is interesting, two microwave sources are utilized along with two harmonic mixers. If the two microwave signals differ in frequency by a small step (typically 10 MHz), then this difference will also get multiplied as the harmonic number goes up. We can use the SIS junction to mix the waves and convert the millimeter waves to signals at various beat frequencies. Finally the signal locked to the harmonic beat frequency can be detected and this selects out the correct harmonic number. This method guarantees the signal to be at the precise frequency without confusion.

To be precise, suppose f_1 and f_2 are two basic microwave frequencies between 10 and 20 GHz. Let $\Delta f = f_1 - f_2$ be small, on the order of a few MHz. After harmonic mixers, signals of frequencies $n_1 f_1$ and $n_2 f_2$ ($n_1, n_2 = 1, 2, 3, \dots$) result with their amplitudes being $A(n_1 f_1)$ and $A(n_2 f_2)$. Some of these waves get attenuated during the transmission from the radiation source to the mixer and are eliminated from the spectrum (for example, those that are below the cutoff frequency of the waveguide). The remaining waves are detected by the SIS mixer, and each wave of frequency f will generate another spectrum of signals of harmonic multiple frequencies mf , $m = 1, 2, \dots$. The overall mixer output is the non-linear mixing results of all the spectrums generated by each wave. Now the final signal is observed with the phase locked to $N\Delta f$, N being a pre-selected number. According to mixing principle, this signal must have components whose frequencies obey $\sum_{i,j} (\pm m_i n_j f_j) = N\Delta f$ where (i, j) are indices of various components of mixing. With our experiment setup N is so chosen that the only suitable components are $m = 1$ and $n_1, n_2 = N$, i.e. only two components are involved. For this particular “beat”, the observed signal *amplitude* is proportional to

$$C_1 A(Nf_1) C_2 A(Nf_2) \approx C^2 I \left(\frac{Nf_1 + Nf_2}{2} \right) \quad (3.4)$$

where C_i , $i=1,2$, are amplitude transmission coefficients from the radiation source to the SIS junction, and I is the intensity of the radiation at source.

This setup of the radiation source is designed to solve the radiation impurity problem. Since we use phase reference method to select out the correct frequency, the signal is guaranteed to be clean. Furthermore, the actual experimental instruments to generate this radiation has the additional advantage of wide frequency range and easily controllable remotely via a GPIB cable.

The second modification is to insert another SIS junction in the receiver as a reference signal channel, thus enabling one to calibrate the incoming power for the measurement. In the modified setup there are therefore two junctions attached to the same antenna. One junction is put at a fixed length from the open-ended resonator stub in the same manner as that of the first experiment and is used to detect the resonance response. The other junction is used to monitor the power absorbed by the antenna and serve as a reference. Signals on both junctions can be measured separately.

In the ideal situation, the two junctions are completely independent, and as direct detectors they produce signals that are measures of *power* dissipated in the junctions according to Tucker's theory. That is to say, in the case of single-frequency incoming radiation with amplitude A , the change in the DC bias current of each junction is given by

$$\Delta I_i = R_i * (C_i A)^2 \quad (3.5)$$

where C_i is the amplitude transmission coefficient from input to junction i and R_i is a constant responsivity for junction i . In the case of multi-frequency “beat” detection, a similar equation for the signal current at the beat frequency holds as discussed above. Therefore by dividing the signals from two channels, the unknown incoming amplitude is eliminated, and we have

$$\frac{I_1(N\Delta f)}{I_2(N\Delta f)} = \frac{R_1}{R_2} \left(\frac{C_1}{C_2}\right)^2 \quad (3.6)$$

This is what the main object to measure in the modified experiment.

In practice, since each junction needs to be DC biased and the convenient bias circuits only permit one single bias wiring, some additional circuits must be constructed to isolate the two junctions effectively. This is discussed in more detail in the following section.

5. Modified Experiment: Setup

The radiation source of the second experiment is shown in Figure. The two microwave sources are both Rohde & Schwarz synthesizers model 309, with calibrated output 12-18 GHz up to 10 dBm. To obtain ample power, an additional RF amplifier (HMMC-5618) for 6-20 GHz is used with each synthesizer to bring the RF level above 10 dBm. The actual power level used for a typical experiment (constant reading on the synthesizer) is measured and is shown in Fig (3.4). Since the WM harmonic mixers (Pacific Millimeters) have roughly more than -30 dB insertion loss for frequency multiplication to around 100 GHz, the required input RF levels are quite high in practice.

The multiple frequency channels coming out of the harmonic mixer are combined via a waveguide “T”, and are filtered with several waveguides to cutoff undesired side frequencies before the millimeter wave power gets radiated out via

a horn. A plastic lens is still used along with the horn to focus the radiation beam into the receiver pattern.

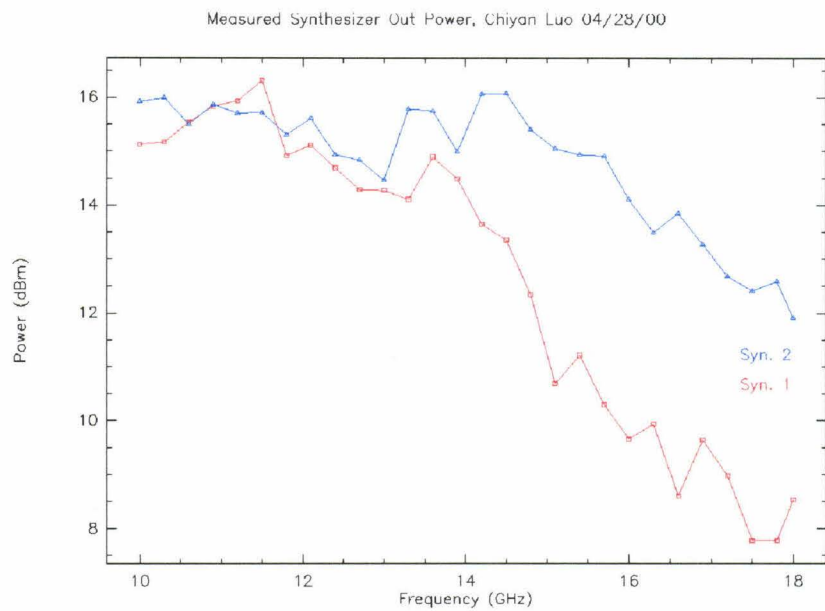


Figure 3.4: Output of the Amplified Microwave Source for a Typical Experiment

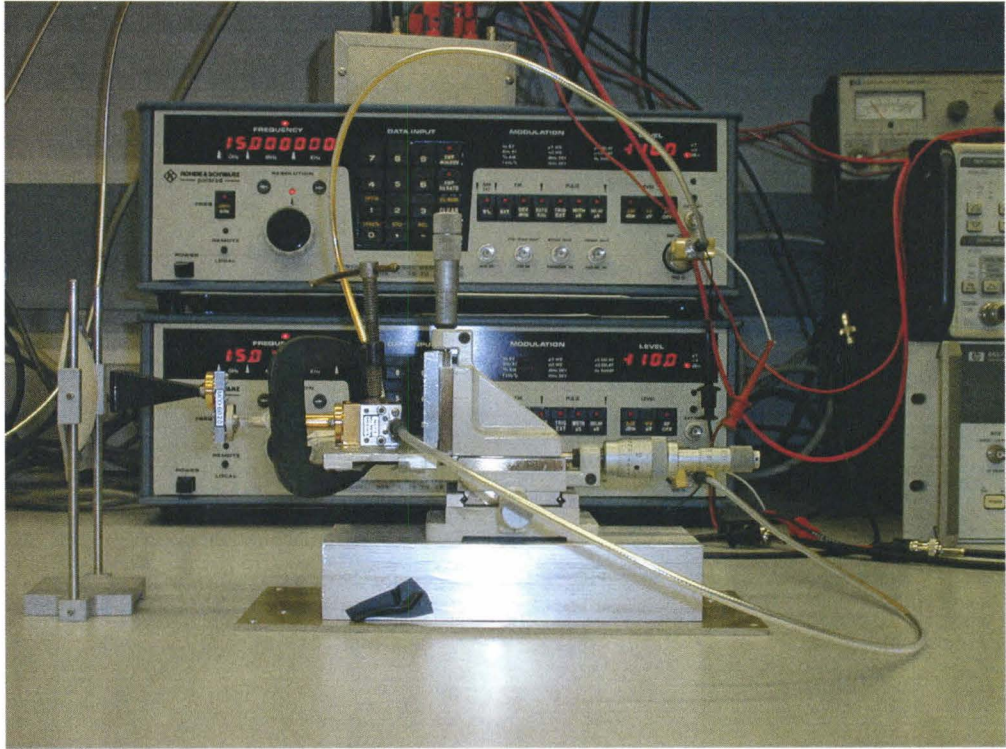


Figure 3.5: Modified Radiation Source Setup

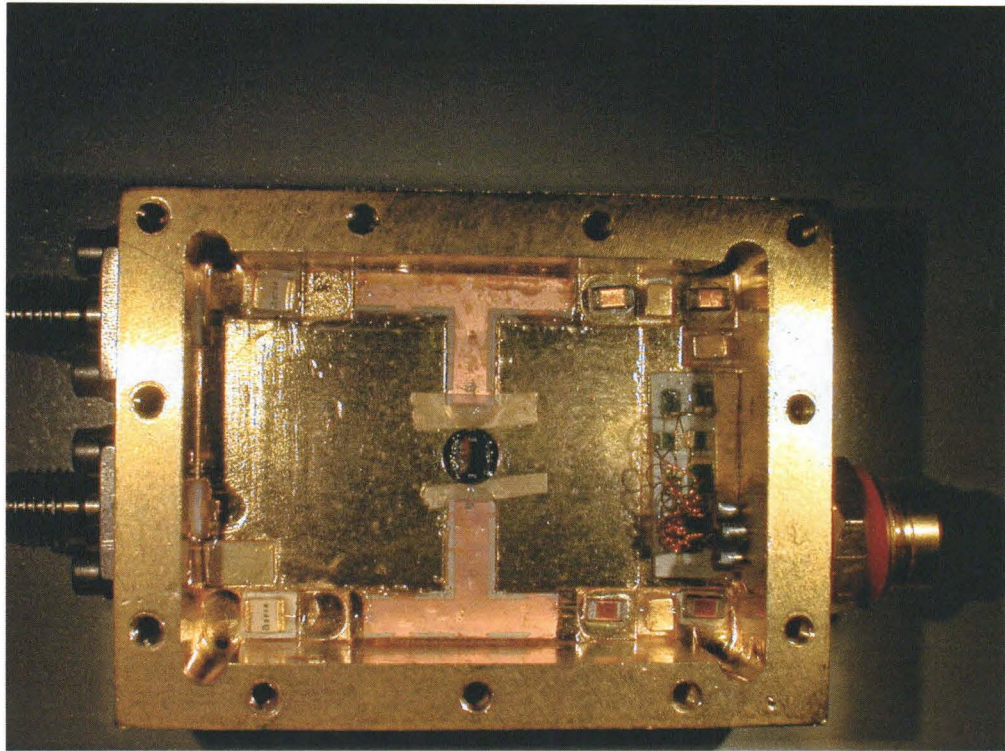


Figure 3.6: New Mixer Block with Bias and Isolation Circuit

For the receiver, a major concern after addition of a second junction is its isolation from the first one. Since the detected signals are at MHz frequency range, construction of direct isolation circuits in the common bias to the two junctions is possible. We finally decided to use simple lumped elements of inductors and capacitors of intermediate values to form the MHz isolation circuits. In practice, the actual circuits that can provide almost perfect isolation are designed to be multi-stage LC dividers, shown in Fig. Because of the new dimension requirements for the additional lumped elements, a new mixer block is designed to house the isolation circuits for simultaneous bias of two junctions as well as the two junction-output ports. This new mixer block is machined at the Physics Shop on Caltech campus. After the new biasing circuits and wirings are installed in the new mixer block, the isolation between two ports are measured

experimentally by injecting 60 MHz radio signals into one port and observing the output on the other port. Without the chips connected the isolation is about -60 dB between two channels around the desired beat frequency 60 MHz, which corresponds to -30 dB isolation before the SIS junctions according to the square law in equation (3.6). The experimental data is plotted on Figure 3.7.

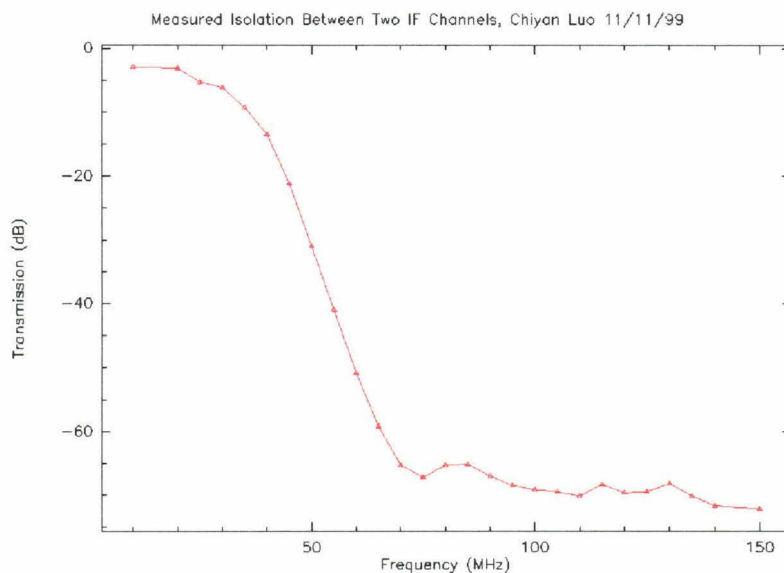


Figure 3.7: Measured IF Isolation Without Chip

The on-chip design of the new device is much like that used in the first experiment. With two junctions in the experiment, only one slot-antenna is used for design simplicity. Radiation power is coupled to the two SIS junctions in opposite polarity via radial stubs and a series of microstrip transformers. The junction without the long stub transmission line sits at the end of the section, while the other junction connects to the open-ended long stub directly. The DC bias pads of the two junctions are on the two sides of the chip, and the two

junctions share a common ground plane. The 80 MHz beat signal is coupled out via the DC bias pads on the chip and connects to the isolation circuits and output ports in the mixer block directly.

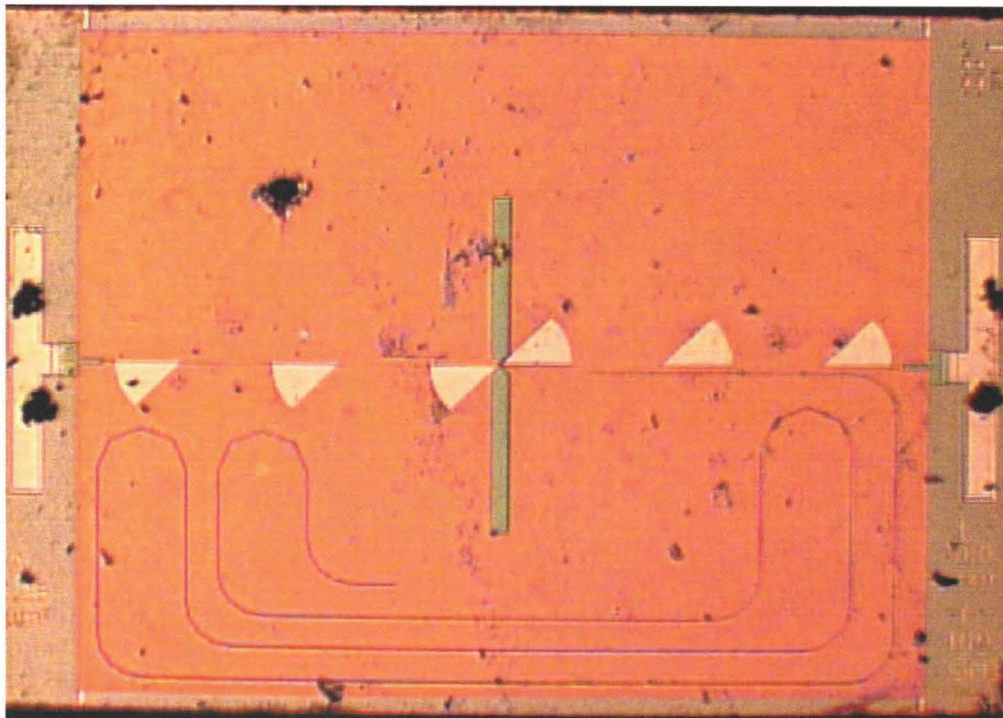


Figure 3.8: A Tested Device for Modified Two-Junction Experiment

With the mixer chip connected in the circuit, it is hard to measure the isolation since we have to use a much weaker signal. The isolation is measured to be roughly -40 dB in 50-60 MHz using a lock-in, corresponding to an actual isolation of -20 dB between the two SIS junctions. This measurement is not very accurate since the RF lock-in noise floor has been reached. The data and the remarks regarding this isolation measurement are presented later in Chapter 4.

The assembled diagram of the modified experiment is shown in Figure (3.9). A signal generator (Hewlett Packard, Model 8657A) has been used as a master clock to synchronize the two microwave synthesizers and generates the difference

beat frequency signal as the radio-frequency lock-in reference signal. As the RF-lockin (Stanford Research Systems, Model SR844) has only one input channel on the panel, a coax-switch is utilized to facilitate the measurement of signals from two channels. This switch is operated by a digital impulse of ± 5 volts and can thus be controlled either through a manual switch, or remotely through an A/D unit which can in turn be operated remotely via GPIB cables. Depending on the controller of the switch, the whole experiment setup is either operated manually or automated by a Linux computer.

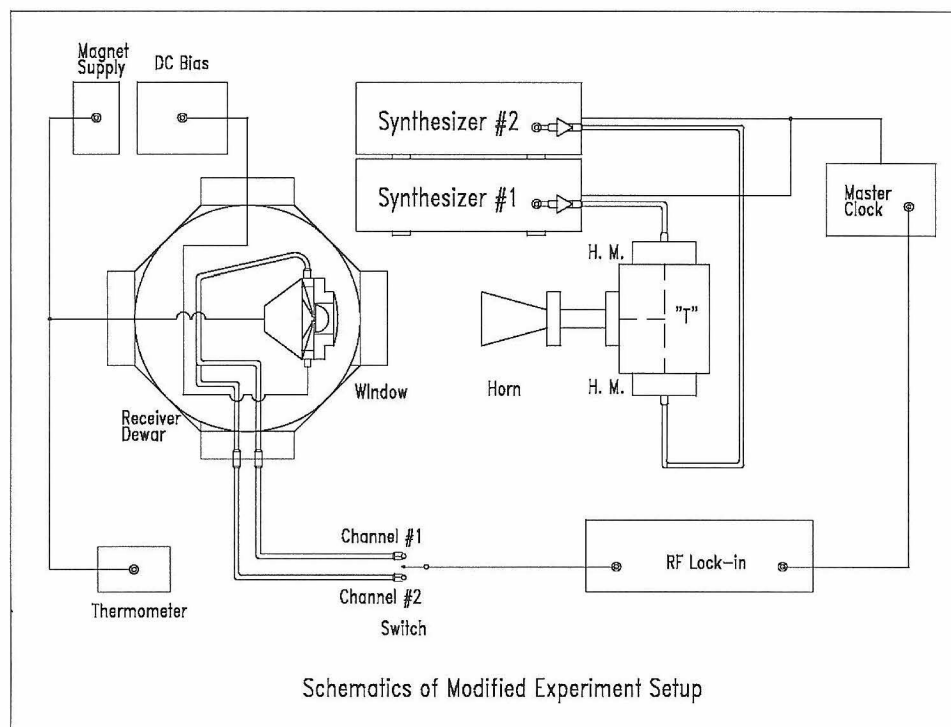


Figure 3.9: Modified Experiment Setup Assembly

6. Modified Experiment: Current Results

The manual version of the modified experiment system was constructed by the end of February 2000 and efforts since then were devoted to optimization of

the data. It is found that the sideband signals in the detector can be strong enough to saturate the SIS junctions, and thus as few sidebands as possible are preferred in the experiment. The complete automated system of the experiment were set up by middle April 2000. The data reported on this section of the thesis were obtained using the automated system.

The modified experiment setup has successfully overcome the signal purity problems in the first experiment. The response in the microstrip resonances is clean and smooth, with resonance nulls correctly spaced and showing the expected shift upon cooling. However, as of the time of this writing, no measurements on the modified system have yet achieved the very deep nulls as was observed in the first experiment, due to SNR limitations. This is rather to our disappointment. } !

Here we report one of the best measured data on a 10mm stripline near 80 GHz. This data set was measured using the fifth harmonic output of the harmonic mixers and 15-17 GHz output of the microwave synthesizer. The two SIS junctions in parallel have a combined normal resistance of 4.9Ω and a combined subgap to normal ratio of roughly 10. The junctions are biased at a constant combined voltage of 2.50mV through the experiment. The combined leakage current at 4.2K is roughly $59\mu\text{A}$ and drops to $45\mu\text{A}$ upon cooling to 1.6K. The data were obtained through several runs of the system, first across the whole band, then in finer steps on the null positions. The measured data is plotted in the following Figure (3.10).

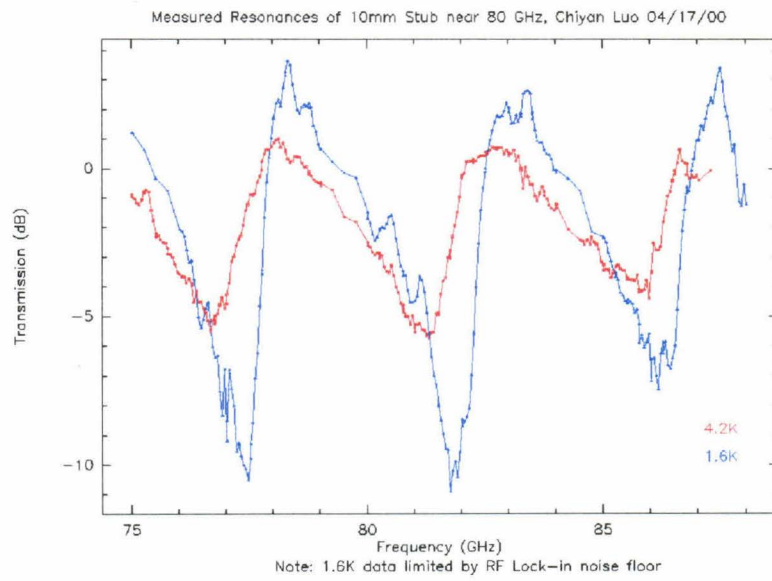


Figure 3.10: Modified Experiment Current Results

Chapter 4

DISCUSSIONS AND CONCLUSIONS

1. Implications of Two Experiments

Our initial experiment shows that the loss in the superconducting striplines could be merely limited by superconductivity even at millimeter wavelengths. If this data is interpreted naïvely, the 30dB null at 1.7K shown in Figure (3.3) is a verification of our initial guess that the dielectric layer in these striplines is strikingly lossless, as shown in the following Figure (4.1). In this figure, a direct simulation fit of the data shows that the approximate upper limit of loss tangent of the dielectric layer is as low as 4×10^{-4} at 1.7K near 100 GHz.

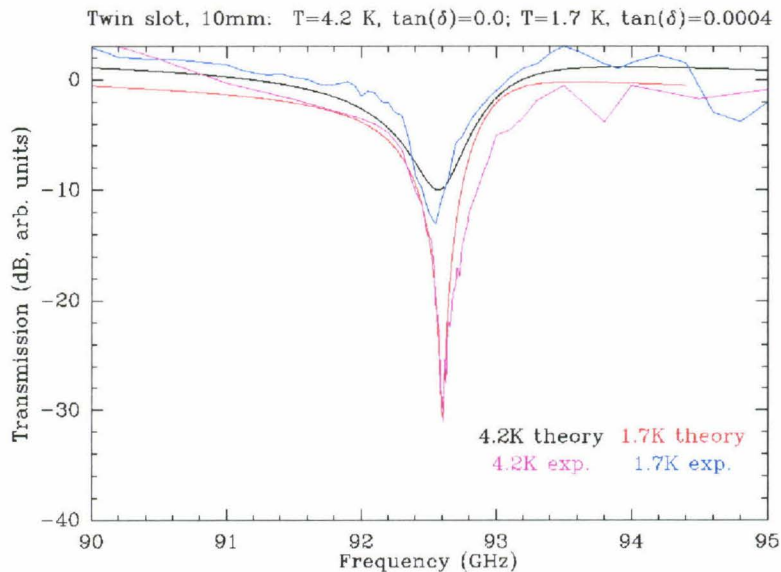


Figure 4.1: Simulation Fit of Basic Experiment Data

Unfortunately, this basic experiment was done with neither input power calibration nor frequency filtering. As can be seen from the simulation, there are some systematic errors that between the experiment data and the simulation fit that cannot be reconciled by adjusting transmission and frequency calibration. One thus has good reasons to suspect that the data may not be a true representation of the microstrip response.

On the other hand, the modified experiment has not yet given the expected response that is similar to the initial experiment. In fact, if the modified experiment results were also interpreted naïvely, we would have a rather lossy transmission line. This is shown in the following simulation fit of the data in Figure (4.2):

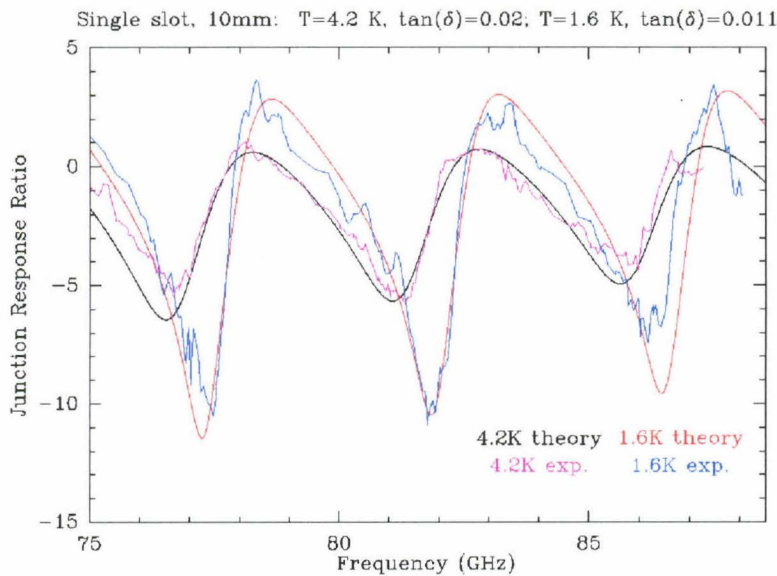


Figure 4.2: Simulation Fit of Modified Experiment Data

The upper limit estimate of the dielectric loss tangent in the superconducting striplines given by the naïve simulation of the data in Figure (4.10) is fairly high, about 0.01 – 0.02. This would necessarily imply that the effect of superconductivity was buried in the dielectric loss, and the performance of the superconducting striplines was in turn limited by its dielectric layer. It would then seem that our initial guess about these transmission lines was incorrect.

Nevertheless, we suspect this direct interpretation of the modified experiment to be not valid in all its aspects, either. One chief reason is that our data at both 4.2K and 1.6K are limited by the signal to noise ratio of the RF lock-in floor, discussed in the next section. The other reason is that we believe that loss in the dielectric to be essentially temperature-independent under our experimental conditions, and thus we trust that the increase in the null depth to be a true signature of superconductivity. The shift in the resonance frequency is also a superconductor characteristic. According to Equation (2.6) this is due to the change in the surface reactance of the superconducting films. Therefore, we believe that we are actually seeing the effects of superconductivity in the modified experiment setup, and it is still possible that our initial guess of lossless dielectric can be true.

2. Limitations of Current Modified Experiment

The modified experiment was designed to eliminate impure frequency components and uncertainties concerning the quasi-optical coupling from the horn to the antenna. Judging from the data, this design goal has been achieved quite confidently on the level of 15 dB. However, some additional difficulties associated with the new technique arise in the experiment. The most prominent obstacle is the limitation imposed by the RF lock-in noise floor, which can be clearly seen in the following figure for the 1.6K data:

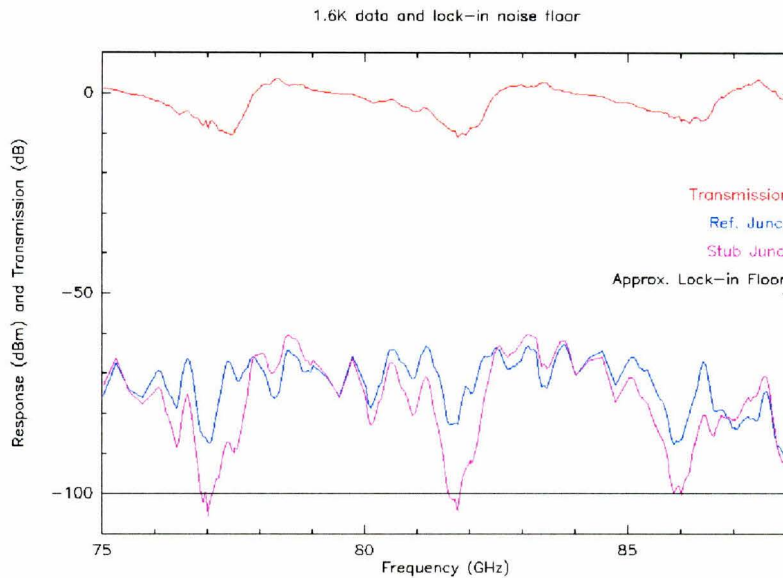


Figure 4.3: 1.6K Data and Lock-in Noise Floor.

The minimum signal that RF lock-in can measure accurately in our IF frequency (50MHz) is in the range from -90 to -100 dBm. Below this level, the fluctuation in the lock-in reading is very significant, indicating that noise interferes with the signal strongly. Thus the depth of the nulls in the measured 1.6K data is limited by the signal-to-noise ratio at the bottom of the RF lock-in. A similar situation also happens at 4.2K where, because of the elevated temperature, all junction response levels are further reduced, and the null levels of all junctions are still hitting the lock-in noise floor. To overcome this difficulty, a possible direction is to use some IF amplifiers to amplify the signal before the lock-in, so that the signal strength is raised appreciably above the floor level.

A second limitation is the intrinsic isolation between the two junctions on chip provided by the mixer block isolation circuit and by the on-chip

superconducting circuits. Currently, the IF isolation circuit is -40dB around 50MHz and -60dB around 60MHz , and the measured isolation after the chip has been connected is at least -40dB . The exact value of the isolation after the chip has been connected has not been accurately measured, since the RF lock-in noise floor level is again being pushed during the isolation measurement. Judging from the data, the isolation stays on -40dB level for most IF frequencies that are greater than 40MHz . This corresponds to at least -20dB isolation between the two junction detectors, and the main limitation seems to come from the on-chip circuit. Therefore, if we wish to measure nulls that are deeper than -20dB in the superconducting transmission lines, further isolation is probably needed in the chip design. This assertion is yet to be confirmed when IF amplifiers are available.

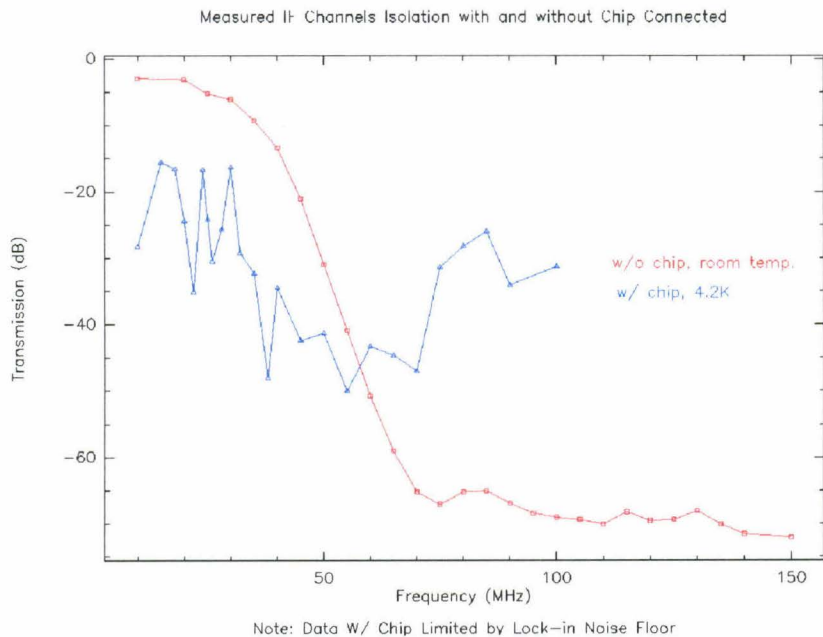


Figure 4.4: Measured IF Channel Isolation with and without Chip

3. Conclusive Remarks and Future Work Directions

At the time of this writing, the only conclusion that can be drawn from our experiments is **the upper limits of the loss tangent of dielectric layer:**

$$\tan(\delta) \leq 0.02 \text{ at } 4.2\text{K} \quad (4.1)$$

and

$$\tan(\delta) \leq 0.011 \text{ at } 1.6\text{K} \quad (4.2)$$

for millimeter wavelength applications near 80 GHz. We also conclusively established that our model for superconducting transmission lines is accurate for phase propagation. We are still uncertain that the loss in our superconducting striplines is mainly limited by dielectric loss or by superconductor loss, and further experiments are necessary to establish the exact answer.

The most promising way of continuing our experiment would be to use some IF amplifiers to obtain sufficiently large signals, so that the RF lock-in noise floor will not be encountered. Moreover, the SIS junctions can be easily saturated if all harmonic components of the radiation are allowed to enter the mixer. Thus some frequency filtering in our source will be a very good idea. Our experiments can also be easily extended to higher frequencies (200 GHz and above) with a change to harmonic mixers in that range.

Future work directions for measuring the loss will need to use a clean power source and include a method for power calibration. Our harmonic radiation generator is a feasible power source, but proper filtering in frequency should be used to prevent the junctions from saturating. On-chip power calibration proves to be a successful way in our experiments, provided that the isolation between two channels is sufficient for the measuring range. In general, accurately

measuring the loss in superconducting striplines in millimeter and submillimeter wavelengths using our method is very possible.

BIBLIOGRAPHY

- J. Bardeen, L. N. Cooper, and J. R. Schrieffer, "Theory of Superconductivity", *Phys. Rev.*, vol. 108, No. 5, pp 1175-1204, 1957.
- Mei Bin, "Low-Noise THz Niobium SIS Mixers", Ph.D. thesis, California Institute of Technology, 1997.
- J. E. Carlstrom, R. I. Plambeck and D. D. Thornton, "A Continuously Tunable 65-115 GHz Gunn Oscillator", *IEEE Trans. Microwave Theory Tech.*, vol MTT-33, No. 7, pp. 610-619, 1985.
- J. Carlstrom and J. Zmuidzinas, in *Review of Radio Science 1993-1996*, edited by W. R. Stone (Oxford University Press, Oxford, 1996), pp. 839-882.
- R. L. Kautz, "Picosecond pulses on superconducting striplines", *J. Appl. Phys.*, 49(1), pp. 308-314, 1978.
- B. W. Langley, S. M. Anlage, R. F. W. Pease, and M. R. Beasley, "Magnetic penetration depth measurements of superconducting thin films by a microstrip resonator technique", *Rev. Sci. Instrum.*, 62(7), pp.1801-1812, 1991.
- D. C. Mattis and J. Bardeen, "Theory of the Anomalous Skin Effect in Normal and Superconducting Metals", *Phys. Rev.*, vol 111, No. 2, pp. 412-417, 1958.
- Thomas G. Phillips and Jocelyn Keene, "Submillimeter Astronomy", *Proc. IEEE*, vol. 80, No.11, pp 1662-1678, 1992.
- A. B. Pippard, *The Dynamics of Conduction Electrons*, New York, Gordon and Breach, 1965.
- Ralf Popel, "Measured Temperature-Dependence of Attenuation Constant and Phase Velocity of a Superconducting PbAu/SiO/Pb Microstripline at 10GHz and 30GHz", *IEEE Trans. Microwave Theory Tech.*, vol. MTT-31, No. 7, pp 600-604, 1983.
- G. E. H. Reuter and E. H. Sondheimer, "The theory of the anomalous skin effect in metals", *Proc. Roy. Soc. (London)*, A195, pp. 336-364, 1948.
- J. P. Turneaure and I. Weissman, "Microwave Surface Resistance of Superconducting Niobium", *J. Appl. Phys.*, vol. 39, No. 9, pp. 4417-4427, 1968.
- John R. Tucker and Marc J. Feldman, "Quantum Detection at Millimeter wavelengths", *Rev.*

Mod. Phys., Vol. 57, No. 4,
October 1985.

J. Ward, F. Rice, G. Chattopadhyay,
and J. Zmuidzinas, "Supermix: A
Flexible Software Library for
High-Frequency Circuit
Simulation, Including SIS Mixers
and Superconducting Elements",
appeared in *1999 Proceedings, Tenth
International Symposium on Space
Terahertz Technology*.

J. F. Whitaker, R. Sobolewski, D. R.
Dykaar, T. Y. Hsiang and G. A.
Mourou, "Propagation Model for
Ultrafast Signals on Superconducting
Dispersive Striplines", *IEEE Trans
Microwave Theory Tech*, vol. 36, No.
2, pp. 277-285, 1988.

J. Zmuidzinas and H. G. LeDuc,
"Quasi-Optical Slot Antenna SIS
Mixers", *IEEE Trans. Microwave
Theory Tech.*, vol. 40, No. 9, pp.
1797-1804, 1992.